Development of a 3D City Model-Based System for Pre-Flight Evaluation and Optimization of Aerial Image Acquisition Plans

Lixian Zhao [1], Saki Kato [1], Kenta Imai [1], Maki Itazu [1], Aya Matsui [1]

[1] Kokusai Kogyo Co., Ltd., 2-24-1 Harumi-cho, Fuchu-shi, Tokyo 183-0057, Japan - {reikan_cho, saki_kato, kenta_imai, maki_itazu, aya_matsui}@kk-grp.jp

Keywords: Flight planning, 3D city model, Pre-flight simulation, Occlusion, Aerial photogrammetry.

Abstract

In dense urban environments, aerial image acquisition often suffers from occlusions and redundant data due to the lack of quantitative evaluation tools at the flight-planning stage. To address this issue, this study develops a flight-planning support system that enables pre-acquisition visibility analysis for both terrain and building surfaces using existing 3D city models. The system performs ray-casting simulations based on user-defined flight parameters to quantify and visualize occluded and visible regions before flight, allowing planners to evaluate data quality and optimize image acquisition efficiency. Experiments were conducted using real flight plans with two representative aerial cameras: the Leica CityMapper-2 for multi-directional texture mapping and the Vexcel UltraCam Eagle 4.1 for nadir-based topographic mapping. The results show that the system effectively visualizes occlusions on roofs and walls, predicts building lean in nadir imagery, and assesses the influence of overlap ratios on ground visibility. These analyses enable users to design more cost-effective and geometrically consistent flight plans by identifying redundant overlaps and ensuring sufficient coverage for DSM and true-orthophoto generation. The proposed framework provides a quantitative and objective approach to improving the transparency and reliability of aerial survey planning, and it offers a foundation for integrating visibility simulation with subsequent photogrammetric workflows such as surface reconstruction and texture mapping.

1. Introduction

In recent years, the utilization of high-precision 3D city models (particularly those of LOD2 or higher) and true orthophotos has rapidly expanded across various domains such as smart cities, urban planning, infrastructure management, and disaster mitigation. These products enable three-dimensional visualization of urban environments and are expected to play crucial roles in land-use analysis, urban development, regulatory planning, and disaster risk assessment.

In Japan, the Project PLATEAU, led by Japan’s Ministry of Land, Infrastructure, Transport and Tourism (MLIT), has been developing LOD2-level 3D city models for major cities nationwide. As of the end of FY2024, approximately 250 cities have been completed, with a target of 500 cities by FY2027 (MLIT, 2025). The project recommends applying texture images to building facades to represent realistic appearances, highlighting the growing importance of textured 3D city models for future urban management.

However, the quality of these products strongly depends on the conditions of aerial image acquisition. In dense urban areas, occlusions and building relief displacement can degrade both geometric and visual quality. Nadir (vertical) images are suitable for producing geometrically stable orthophotos but often fail to sufficiently capture ground surfaces, resulting in DSM inaccuracies and missing areas in true orthophotos. Conversely, oblique imagery can directly capture building facades and has proven effective for texture generation in LOD2 modeling.

Numerous studies have demonstrated the advantages of oblique imagery. Ishikawa et al. (2025) compared texture images generated from nadir and oblique photographs and demonstrated that oblique images enable the extraction of detailed building elements such as doors and windows. Vacca et al. (2017) conducted UAV flights using both nadir-only and combined nadir + oblique imaging, showing that the integration of oblique images significantly increased point cloud density and improved measurement accuracy in building height, area, and volume. Furthermore, Buyukdemircioglu and Oude Elberink (2024) developed an automated texture-mapping system for CityJSON models, demonstrating high-quality texture generation from combined nadir and oblique aerial images.

However, the use of oblique imagery introduces two major challenges: (1) frequent occlusion in dense urban environments, and (2) increased data volume due to multi-directional camera systems. Since these two factors are in a trade-off relationship, reducing occlusions generally requires additional flight lines and images, which leads to higher operational costs. Therefore, optimizing flight planning by balancing occlusion reduction and data volume control is essential.

Figure 1. Occlusions in an oblique image

This contribution has been peer-reviewed. The double-blind peer-review was conducted on the basis of the full paper.
https://doi.org/10.5194/isprs-annals-XI-2-2026-419-2026 | © Author(s) 2026. CC BY 4.0 License.

Occlusions occur more frequently in oblique images than in nadir images. Additionally, occlusion would be unavoidable in texture mapping of building surfaces in a built-up area. Figure 1 illustrates an oblique image that exhibits occlusions.

In Japan, aerial oblique images for texture mapping are typically collected using multi-directional camera systems. In a multi-directional camera system, the volume of data collected simultaneously by the nadir and oblique cameras can be large. Not all collected oblique images are used for texture mapping. Figure 2 shows a sample of the coverages of oblique images taken by the Leica CityMapper-2 (CM-2). The grey level in Figure 2 indicates the number of overlaps of images, such as the brighter tones indicate higher overlap levels, and the white region is not photographed. The blue rectangle in Figure 2 indicates the target area for texture mapping.

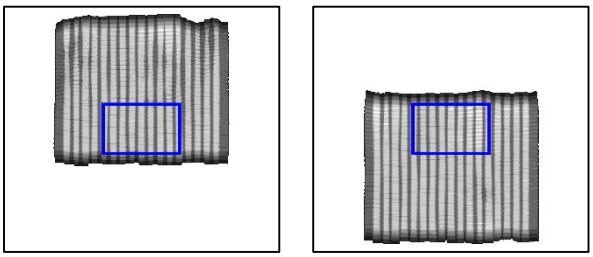

(a) Forward camera (b) Backward camera

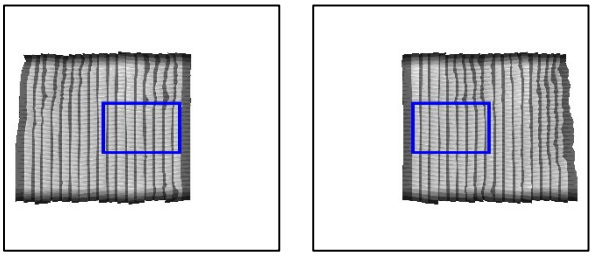

(c) Leftward camera (d) Rightward camera

Figure 2. Coverages of oblique images captured for texture mapping of the blue rectangle area

Existing flight-planning software is typically designed for nadir imaging, focusing on parameters such as overlap ratios and ground sampling distance (GSD). As a result, it cannot adequately evaluate occlusions or relief displacement that occur in oblique images, making it difficult to predict the quality of the final products during the planning stage. To address these challenges, this study develops a software system designed to assist image collection planning, enabling pre-evaluation of data quality at the flight-planning stage using existing 3D city models. The system accepts user-defined flight parameters (altitude, camera tilt, end lap and side lap ratios, etc.) and performs ray-casting simulations to quantify and visualize ground and wall visibility, occlusion distribution, and the degree of building relief displacement. It should be noted that the proposed system does not automatically generate flight plans; rather, it supports planners by providing quantitative visibility and occlusion analyses to improve the quality of final data products before acquisition.

This study focuses on three operational challenges: (1) improving texture quality by optimizing the trade-off between occlusion and data volume in multi-directional image collection; (2) enhancing ground visibility and reducing occlusion in nadir image planning to ensure geometric precision in DSM and true-orthophoto generation; and (3) predicting building relief displacement to support geometric planning of image acquisition. Through these investigations, the study proposes a quantitative framework for evaluating aerial image acquisition plans and demonstrates its practical applicability through real-world case studies.

2. Related Work and Current Image Collection Planning

Research focused on improving flight planning for aerial photogrammetry remains limited. In most current photogrammetric workflows, even when multi-directional camera systems are adopted, the flight plan is still designed in essentially the same manner as for traditional nadir cameras, based primarily on GSD, end lap (EL), and side lap (SL) ratios. Such planning focuses on geometric consistency and image matching, while occlusions in complex urban environments are generally not evaluated. Consequently, the resulting datasets often suffer from visibility gaps in dense city areas, leading to incomplete DSMs or missing facade textures in 3D modeling.

Alfakhori et al. (2022) proposed an “Occlusion Screening” method that utilizes existing 3D city models as a reference database to automatically extract occluded regions. Their method provides a useful framework for visualizing invisible areas in mobile AR and urban visualization applications. However, this approach focuses primarily on identifying occluded spaces in a static context rather than integrating occlusion information into the flight-planning process. In contrast, the present study aims to incorporate occlusion analysis directly into the design phase of aerial image acquisition. By calculating commonly occluded regions across multiple viewing directions and linking them to specific flight parameters, the proposed method enables pre-evaluation and optimization of flight plans for practical applications such as UAV-based urban mapping.

Optimizing flight plans by balancing occlusion reduction and data volume remains a key operational challenge. Traditional flight-planning systems primarily target nadir imagery and rely on fixed overlap and GSD settings without assessing visibility performance. Although recent studies (e.g., Ishikawa et al., 2025; Gajski & Dzięgielewska-Gajski, 2023) have emphasized the importance of balancing occlusion and data volume when using multi-directional camera systems, few existing systems are capable of quantitatively evaluating visibility and occlusion distributions using 3D city models. This study addresses that gap by developing an evaluation software system that links flight parameters to visibility and occlusion metrics derived from 3D city data, thereby enabling more effective pre-evaluation of data quality in aerial survey planning. The following section outlines the processing flow and core functions of the developed system for assisting image collection planning.

3. Outline of the Processing of the Developed System for Assisting Image Collection Planning

3.1 Image Collection Planning Using the Developed System

The developed system does not automatically design an image collection plan but provides information to assist image collection planning. The procedure for the image collection plan using the developed system is as follows:

1) Conduct ordinary image collection planning and obtain the positions and attitudes of the cameras.
2) Provide the obtained camera positions and attitudes, 3D city model data, and a DEM to the developed system.
3) Obtain some information for assisting image collection planning from the system.
4) Determine whether the current image collection plan is

satisfactory for the designated purpose.

5) If the current image collection plan is satisfactory, finish the image collection planning; otherwise, modify the current plan and go to Processing 2).

3.2 Processing Flow of the Developed System

The processing of the developed system basically consists of two parts. The first part determines the visible regions on building and terrain surfaces. The second part provides information to assist image collection planning based on the results of the first part. Figure 3 shows the process flow of the developed system.

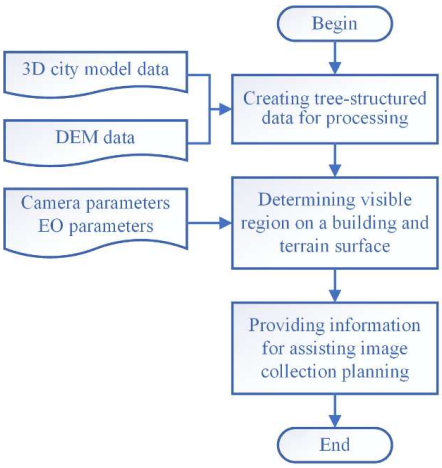

Figure 3. Process flow of the developed system

3.3 Determining Visible Region on a Building and Terrain Surface

Determining the visible regions on building or terrain surfaces in urban areas with densely distributed buildings is a highly time-consuming task.

3.3.1 Basic Idea: There are two ways to determine whether a point on a building or terrain surface is visible from a camera. One is based on the idea that “whether we can see the camera or not” indicates “whether we are photographed by the camera or not.” The other is based on the idea that “whether the camera sees us or not” indicates “whether we are photographed by the camera or not.”

The former idea can be implemented using ray tracing or a hemispherical viewshed, which represents the angular distribution of sky obstruction. Figure 4 shows a hemispherical viewshed, which is a fisheye lens image viewed from a point on the earth. The method based on the former idea is referred to as “Method A” in this paper.

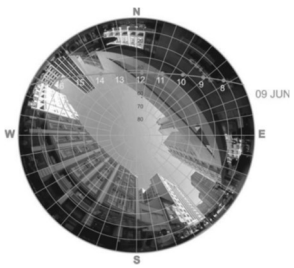

Figure 4. Fisheye image viewed from a point on the earth (Minella et al., 2011)

In contrast, the latter idea can be implemented using projection images viewed from a camera. The latter idea was adopted by Matsuoka et al. (2024) for determining sunshine region of building surfaces in their PV potential estimation system. We call the method based on the latter idea "Method B" in the paper. From now on, we discuss the algorithm to determine the visibility on a building surface. The algorithm on a terrain surface is the same as that on a building surface.

Figure 5 shows an aerial image collected by an oblique camera with an off-nadir angle of 45°. Figure 6 shows a projection image corresponding to the real aerial image shown in Figure 5. The projection image in Figure 6 is created by using a 3D city model and the exterior orientation (EO) parameters of the aerial image shown in Figure 5. Each building surface in Figure 6 is colored according to its ID. From now on, an aerial image corresponding to a projection image is called a target image.

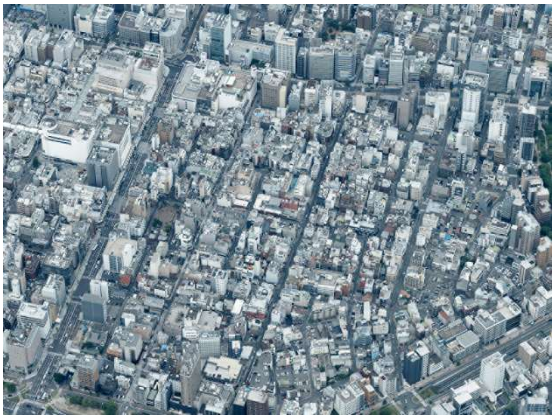

Figure 5. Aerial image collected by an oblique camera with the off-nadir angle of 45°

Figure 6. Projection image viewed by an oblique camera with the off-nadir angle of 45°

Using computer graphics (CG) techniques such as the depth buffer (Z-buffer) algorithm, which does not examine the intersection of the sun ray, can provide projection images viewed by the sun much more rapidly. Additionally, using another CG technique named the scanline algorithm for filling polygons can create a projection image more rapidly.

Roughly speaking, the computation time of Method A is proportional to the square of the number of polygons in the 3D city model, whereas that of Method B is proportional to the number of polygons. However, Method A directly provides the information on the visibility of a point on a building surface,

while a projection image in Method B cannot provide the information on the visibility directly. Method B requires additional processing to determine the visibility of each point on a surface except for producing a projection image. The computation time of the additional processing would be proportional to the number of polygons. Accordingly, Method B is adopted from the viewpoint of computational efficiency.

3.3.2 Image Geometry: Before showing the processing flow of Method B, we discuss the image geometry. The image coordinate system is considered a planar rectangular coordinate system (x, y), while the object space coordinate system is regarded as a spatial rectangular coordinate system (X, Y, Z), as illustrated in Figure 7.

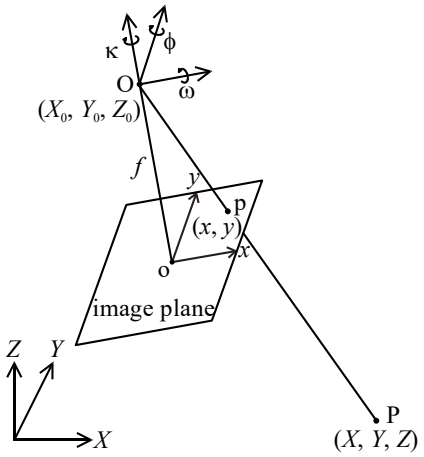

Figure 7. Image coordinate system (x, y) and object space coordinate system (X, Y, Z)

Consider that an image is taken by a camera with focal length f and pixel size δ. (X_O, Y_O, Z_O) and (ω, ϕ, κ) represent the position and attitude of the camera in the object space coordinate system (X, Y, Z). The rotation matrix $R[r_{ij}]$ of the camera is as follows:

$$R = R_\kappa R_\phi R_\omega \tag{1}$$

where

$$R_\omega = \begin{bmatrix} 1 & 0 & 0 \\ 0 & \cos\omega & \sin\omega \\ 0 & -\sin\omega & \cos\omega \end{bmatrix} \tag{2}$$

$$R_\phi = \begin{bmatrix} \cos\phi & 0 & -\sin\phi \\ 0 & 1 & 0 \\ \sin\phi & 0 & \cos\phi \end{bmatrix} \tag{3}$$

$$R_\kappa = \begin{bmatrix} \cos\kappa & \sin\kappa & 0 \\ -\sin\kappa & \cos\kappa & 0 \\ 0 & 0 & 1 \end{bmatrix} \tag{4}$$

Let the point $P(X, Y, Z)$ be projected to the image point $p(x, y)$ on an aerial image. Here the image point $p(x, y)$ is as follows:

$$x = -f\frac{u}{w} \tag{5}$$

$$y = -f\frac{v}{w} \tag{6}$$

where

$$u = r_{11}(X - X_O) + r_{12}(Y - Y_O) + r_{13}(Z - Z_O) \tag{7}$$

$$v = r_{21}(X - X_O) + r_{22}(Y - Y_O) + r_{23}(Z - Z_O) \tag{8}$$

$$w = r_{31}(X - X_O) + r_{32}(Y - Y_O) + r_{33}(Z - Z_O) \tag{9}$$

Here the viewing vector $\vec{V}(u, v, w)$ represents the vector from the exposure centre O to the point P, and w expresses the depth.

Let (c_O, r_O) be the column and the row of the principal point in the image. The column c and the row r of the image point $p(x, y)$ are as follows:

$$c = \frac{x}{\delta} + c_O \tag{10}$$

$$r = -\frac{y}{\delta} + r_O \tag{11}$$

Let $\vec{N}(n_X, n_Y, n_Z)$ be the exterior normal vector of the plane on which a polygon lies. The equation of the plane can be expressed as follows:

$$n_X X + n_Y Y + n_Z Z + d = 0 \tag{12}$$

The incident angle θ of the viewing vector $\vec{V}$ to the polygon can be expressed as follows:

$$\cos\theta = \frac{\vec{N}\cdot\vec{V}}{|\vec{N}||\vec{V}|} = \frac{n_X u + n_Y v + n_Z w}{\sqrt{n_X^2 + n_Y^2 + n_Z^2}\sqrt{u^2 + v^2 + w^2}} \tag{13}$$

The equation $w = F(c, r)$ for calculating the depth w of a pixel (c, r) on the projection image is as follows:

$$w = F(c, r) = \frac{g_1 f}{g_x\delta(c - c_O) - g_y\delta(r - r_O) + g_z f} \tag{14}$$

where

$$g_x = r_{11}n_X + r_{12}n_Y + r_{13}n_Z \tag{15}$$

$$g_y = r_{21}n_X + r_{22}n_Y + r_{23}n_Z \tag{16}$$

$$g_z = r_{31}n_X + r_{32}n_Y + r_{33}n_Z \tag{17}$$

$$g_1 = n_X X_o + n_Y Y_o + n_Z Z_o + d \tag{18}$$

3.3.3 Processing Flow: Method B for obtaining the information on the visibility of a point on a building surface consists of three steps. The first step is the preprocessing step for preparing the following main steps. The second step is the step for producing a projection image, and the third step is the step for determining the visibility of each point using the produced projection images. Figure 8 shows the process flow of Method B for obtaining the information on the visibility of a point on a building surface.

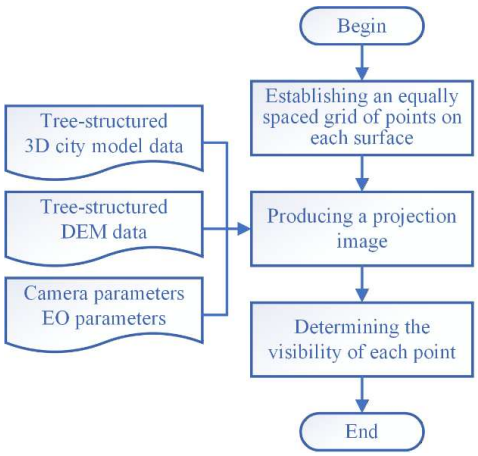

Figure 8. Process flow for obtaining the information on the visibility of a point on a building surface

Step I: preprocessing

1) Establish an equally spaced grid of points on each building surface where the visibility will be determined.
2) Prepare a matrix for storing the number of aerial images photographing each grid. The matrix is called a visibility matrix and is initially filled by 0, as shown in Figure 9.

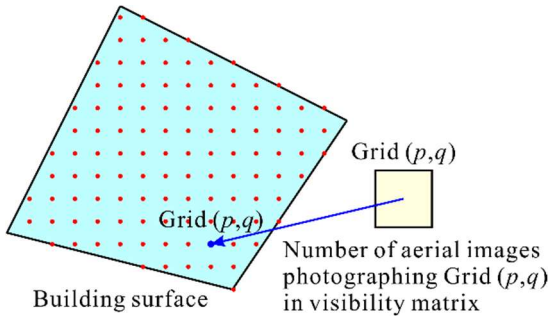

Figure 9. Visibility matrix

Step II: producing a projection image

1) Obtain an equation $w = F(c,r)$ for calculating the depth w of a pixel (c,r) on the projection image as to each polygon on building surfaces of a 3D city model.
2) Prepare two matrices with the same size as the target image for storing intermediate results. One is for storing the polygon ID, and the other is for storing the depth w of each pixel (c,r) of the target image. The former is called an ID matrix, while the latter is called a depth matrix. The structures of the ID matrix and the depth matrix are shown in Figure 10. The ID matrix is initially filled by NULL.

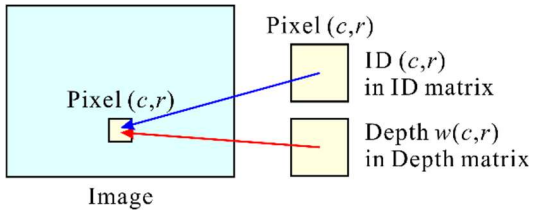

Figure 10. ID matrix and depth matrix

3) Calculate image coordinates (c,r) on the projection image of the vertexes (X,Y,Z) of a polygon of a building surface using the EO parameters $(X_O, Y_O, Z_O, \omega, \phi, \kappa)$ of the target image.
4) Fill the polygon on the temporal projection image with its ID using the scanline algorithm.
5) Calculate the depth w of each filled pixel (c,r) on the projection image using the equation $w = F(c,r)$ derived at first.
6) Store the polygon ID and the depth w of each pixel (c,r) in the ID matrix and the depth matrix, respectively, if one of the following conditions is satisfied:
   a) The polygon ID stored in the ID matrix is NULL.
   b) The polygon ID stored in the ID matrix is not NULL, and the depth in the depth matrix is larger than the calculated depth.
7) Go to Processing 3), if there remain unprocessed polygons; otherwise, producing a projection image storing the polygon IDs is finished. This is the depth buffer (Z-buffer) algorithm.

Step III: determining the visibility of each point

1) Obtain the viewing vector $\vec{V}(u,v,w)$ from the exposure centre O to a grid (X,Y,Z) of a polygon of a building surface using the EO parameters $(X_O, Y_O, Z_O, \omega, \phi, \kappa)$ of the target image.
2) Calculate the incident angle of the viewing vector $\vec{V}$ to the current polygon using the equation of the plane on which a polygon lies. If the calculated incident angle is larger than the predefined threshold, go to Processing 1) as to the next grid for avoiding undesirable results.
3) Calculate the image coordinates (c,r) on the projection image of the current grid.
4) Examine the polygon ID stored in the ID matrix. If the stored polygon ID is the same as the current ID, the current grid of the current polygon is visible; otherwise, the grid is not visible. If the grid is visible, increment the number of images photographing the grid stored in the visibility matrix.
5) Execute Processing 1) through 4) as to every grid of every building.

3.4 Providing Information for Assisting Image Collection Planning

Necessary information for assisting image collection planning varies depending on the purpose of image collection planning. We assumed the following three cases of image collection planning:

a) Image collection planning for texture mapping of a building surface of a 3D city model using a multi-directional camera system.
b) Image collection planning for 2.5D topographic mapping using aerial nadir images.
c) Image collection planning for creating an orthoimage from an aerial nadir image using DEM instead of DSM.

3.4.1 For Texture Mapping of Building Surface of a 3D City Model Using a Multi-Directional Camera System: The system produces an image indicating the proportion of the visible area of a building surface. The image, which is called a building visibility image, is produced as a ground plan. As for roof surfaces, the color of each roof surface indicates the proportion of its visible area. On the contrary, as for wall surfaces, the color of the orthographic projection of each wall surface, which becomes a line, indicates the proportion of its visible area. A building visibility image can be produced easily from the visibility matrix of each polygon of building surfaces.

3.4.2 For 2.5D Topographic Mapping Using Aerial Nadir Images: The system produces an image indicating regions of occlusions. The image, which is called a terrain measurability image, is also produced as a ground plan. Each element of a terrain measurability image represents whether the corresponding grid of the terrain surface can be measured using more than an aerial image or not. A terrain measurability image can be generated easily from the visibility matrix of each polygon of terrain surfaces.

3.4.3 For Creating an Orthoimage from an Aerial Nadir Image Using DEM Instead of DSM: The system produces an image indicating relief displacement of building surfaces. This image, referred to as a wall visibility image, is generated for each target image. A wall visibility image is a sort of projection image. In a wall visibility image, polygons of wall surfaces are colored white, while those of roof surfaces are colored grey. Figure 13 shows a wall visibility image.

4. Experiment

To evaluate the performance and practical applicability of the developed system, experiments were conducted using real flight plans executed in previous aerial survey operations.

4.1 Image Collection Planning for Texture Mapping of Building Surfaces in a 3D City Model Using a Multi-Directional Camera System

In the texture-mapping experiment, we used the Leica CM-2, one of the most widely used aerial camera systems capable of capturing oblique images. The specifications of the CM-2 are shown in Table 1 (Leica Geosystems AG, 2025). Figure 11 shows the ground footprints of a nadir camera and four oblique cameras of the CM-2 (Leica Geosystems AG, 2025).

	CM-2 Nadir
Image size	14,192 × 10,640 pixels
Physical pixel size r	3.76 µm
Lens system focal length f	71 mm
Field of view θ across track × along track	41.2° × 31.5°
Flying height H for 10 cm GSD	1890 m
	CM-2 Oblique
Image size	14,192 × 10,640 pixels
Physical pixel size r	3.76 µm
Lens system focal length f	189 mm
Field of view θ image column × image row	16.1° × 12.1°

Table 1. Specifications of the CM-2
(Leica Geosystems AG, 2025)

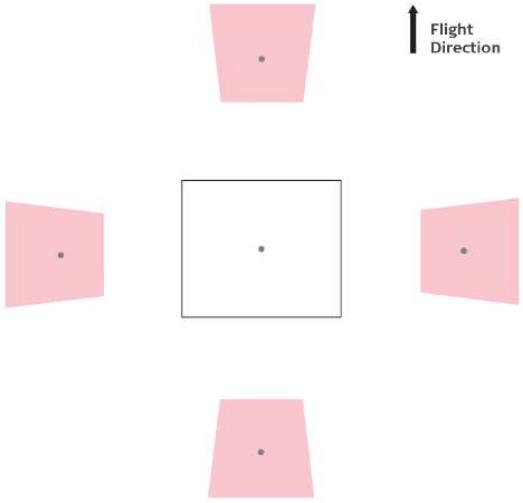

Figure 11. Ground footprint of the CM-2
(Leica Geosystems AG, 2025)

Figure 12 shows the image collection plan for texture mapping using the CM-2. The flight plan used in this experiment covers the area of interest (AOI) in Hiroshima City with both nadir and four-direction oblique cameras. The plan was designed to ensure that all building facades in the AOI were observed from multiple directions. Based on the recorded flight positions, the nadir images were planned with approximately 10 cm GSD, 80% EL, and 60% SL. By using these actual flight parameters in the ray-casting computation, the proposed system assesses the visibility of roof and wall surfaces under realistic acquisition geometry.

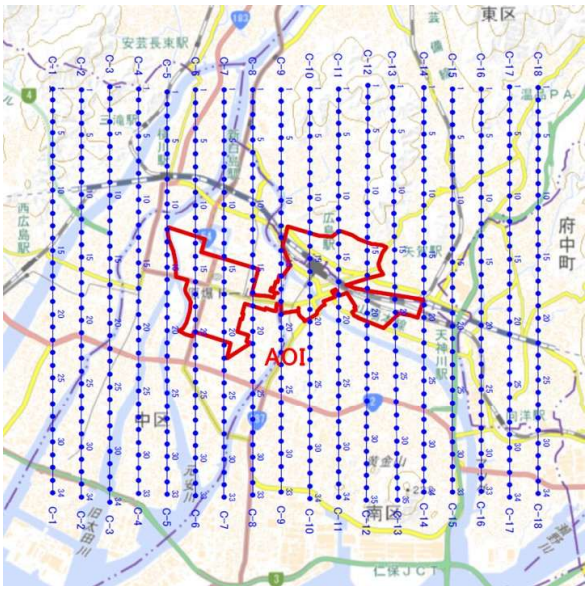

Figure 12. Image collection plan for texture mapping using the CM-2

Figure 13 shows a part of the building visibility image of walls produced by the developed system. As illustrated, occlusions tend to occur at the lower portions of tall buildings and in narrow street canyons where neighboring structures block the line of sight. The spatial distribution of occluded walls can be visually identified, enabling operators to adjust camera tilt or increase flight-line density in advance.

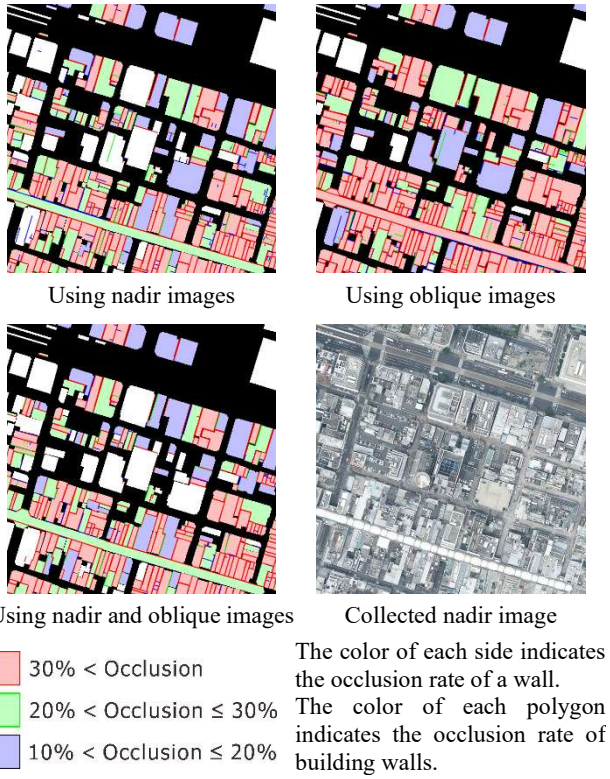

Figure 13. Building visibility image

Table 2 summarizes the image utilization rate and the occlusion rate for the roof and wall surfaces of 4,741 buildings in the AOI. Among the three tested patterns— (1) nadir-only, (2) oblique-only, and (3) total, the total configuration achieved the lowest

occlusion rate. However, its image-utilization rate remains low (35.5%), meaning a considerable portion of collected images do not contribute effectively to facade texturing. By quantifying texture availability and data redundancy, the proposed system supports more cost-efficient planning; unnecessary flight lines can be identified and removed while maintaining sufficient facade coverage.

Camera	Image utilization rate	Occlusion rate	
		Roof	Wall
Nadir	41.1%	1.6%	14.7%
Oblique	34.2%	1.9%	22.1%
Total	35.5%	1.1%	12.7%

Table 2. Image utilization rate and occlusion rate

4.2 Image Collection Planning for Topographic Mapping Using a Nadir Camera

In the experiment as to topographic mapping we used the Vexcel Imaging UltraCam Eagle 4.1 (UCE 4.1), which is a new aerial nadir camera for topographic mapping. The specifications of the UCE 4.1 are shown in Table 3 (Vexcel Imaging, 2025).

	UCE 4.1
Image size	28,110 ×18,060 pixels
Physical pixel size r	3.76 µm
Lens system focal length f	90 mm
Field of view θ across track × along track	60.5° × 41.1°
Flying height H for 10 cm GSD	2410 m

Table 3. Specifications of the UCE 4.1
(Vexcel Imaging GmbH, 2025)

The area of interest is the Shinjuku–Shibuya district in central Tokyo, characterized by dense high-rise buildings. Figure 14 shows the actual image collection plan for topographic mapping using the UCE 4.1. The plan employs parallel flight lines covering the AOI with EL = 80%, SL = 60%, and a nominal GSD of approximately 12 cm, representing typical operational settings for urban DSM and true-orthophoto production.

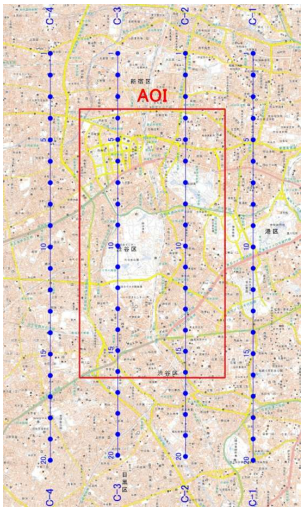

Figure 14. Image collection plan for topographic mapping using the UCE 4.1

Figure 15. Terrain measurability image

4.2.1 Ground-Surface Occlusion Analysis: In this subsection, the developed system was applied to analyze ground-surface occlusions that occur in dense urban areas when using nadir images. Figure 15 shows a terrain measurability image of the AOI produced by the developed system. The yellow regions are captured by a single image, and the red regions are not captured at all. Stereo measurement is not possible in either region.

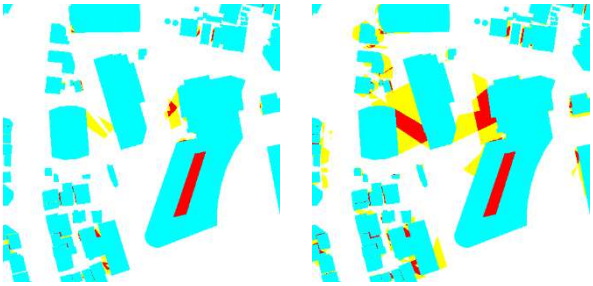

80% EL 60% EL

Figure 16. Terrain measurability image

To evaluate the effect of end lap on ground-surface visibility, a comparative dataset was prepared by thinning the original images—i.e., using every other image along each flight line—to simulate a plan with 60% EL. Figure 16 shows a partial terrain-measurability image for the AOI under both the original (80% EL) and simulated (60% EL) settings. The collected image C-3-05 (Figure 17) would not be acquired under the 60% EL plan; its absence leads to an observable expansion of occluded regions (Figure 16). The figure illustrates how tall buildings in dense districts such as Shinjuku and Shibuya block nadir views and produce unmeasurable terrain areas. The developed system generates comparative occlusion maps (e.g., Figure 16) from ray-casting visibility analysis, enabling users to identify occlusion hotspots pre-flight. This information supports practical adjustments to flight-line layout and overlap settings, providing an objective basis for balancing coverage—and hence geometric completeness—against data-volume efficiency in DSM and true-orthophoto production.

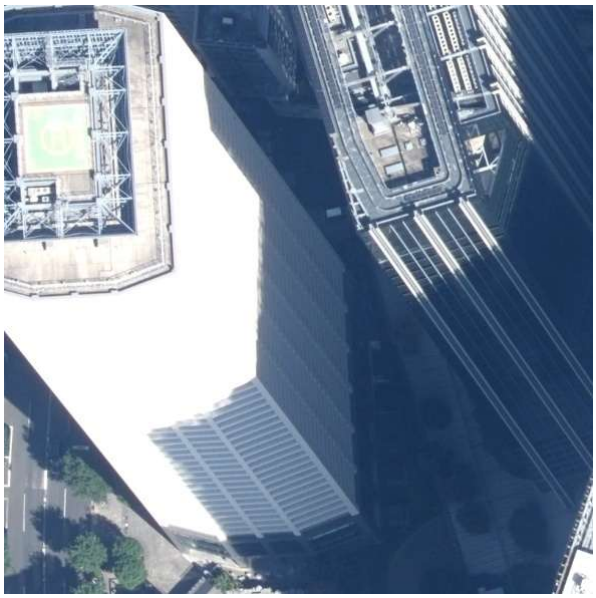

Figure 17. Collected image C-3-05

4.2.2 Building-Lean Prediction: In this subsection, the developed system was used to predict the apparent lean of buildings in nadir imagery. Figure 18 shows a wall visibility image of C-3-06 generated by the developed system, and Figure 19 presents the corresponding collected aerial image. The simulated result successfully predicts how the building appears tilted due to relief displacement, and the collected image confirms a similar direction and degree of apparent lean despite minor differences in the EO parameters.

Figure 18. Wall visibility image of C-3-06

Figure 19. Collected image C-3-06

This comparison demonstrates that the system can forecast the degree of building lean in nadir imagery before flight. Such predictive capability helps operators anticipate which parts of facades will be visible or hidden, allowing them to design more efficient flight plans and ensure sufficient image coverage for accurate modeling. In addition, visualizing predicted lean provides a practical basis for parameter adjustment and for explaining flight plan design to stakeholders. We note that predicting apparent building lean addresses the image-domain manifestation of relief displacement; its actual effect on DSM accuracy depends on the subsequent matching and surface-reconstruction algorithms (e.g., area-based matching may be more sensitive to such distortions than feature-based methods), and is thus outside the direct scope of this study.

Although the proposed system enables iterative refinement of flight plans, a detailed case study demonstrating a fully optimized flight plan has not been included in this paper due to space limitations. This will be addressed in future work, where practical optimization workflows and quantitative comparisons before and after optimization will be presented.

5. Conclusion

This study presented a flight-planning support system that enables pre-acquisition visibility analysis for both terrain and building surfaces. The system performs ray-casting simulations using planned flight parameters and camera geometry to visualize occluded and visible regions, assisting operators in evaluating the effectiveness of image acquisition plans before flight.

Experimental evaluations were conducted using two representative camera systems: the Leica CM-2 for multi-directional texture mapping and the Vexcel UCE 4.1 for nadir-based topographic mapping. The results demonstrate that the developed system can visualize occluded areas on both roofs and walls, predict apparent building lean in nadir imagery, and quantify the influence of overlap ratios on ground-surface visibility. These capabilities enable users to design more efficient and cost-effective flight plans by identifying redundant overlaps while ensuring adequate geometric completeness for DSM and true-orthophoto generation.

The proposed system is designed as a practical alternative to conventional flight-planning methods, with a strong emphasis on computational efficiency for large-scale urban applications. To achieve this objective, the current framework focuses primarily on geometric visibility and occlusion analysis, while other aspects of image quality are simplified or not explicitly modeled.

As a consequence of this design choice, several limitations should be acknowledged. First, the accuracy of the visibility analysis strongly depends on the quality and level of detail of the input 3D city model. In areas where 3D city models are incomplete, outdated, or lack sufficient geometric detail, the reliability of the simulation results may be reduced. In addition, objects that are not explicitly represented in the 3D city model, such as trees or temporary structures, are not considered in the current analysis, which may lead to an underestimation of occlusions in certain environments.

Second, the current system does not evaluate the incident angle between the viewing vector—defined by the projection center and image pixels—and the object surface. As a result, it cannot estimate resolution, which is one of the key components of geometric image quality. Since resolution varies depending on the viewing direction relative to the surface, incorporating this factor is an important direction for future improvement. It is expected that such an extension can be implemented without a significant increase in computational cost.

Finally, radiometric factors such as illumination conditions and shadows are not considered in the present framework. Incorporating these factors would require additional information, including solar position (sun altitude and azimuth), solar irradiance data, and surface reflectance properties (e.g., bidirectional reflectance). Although it is technically possible to include such factors, the associated computational cost would be substantial. Therefore, their integration is considered impractical for a flight-planning support system that prioritizes efficiency.

Despite these limitations, the proposed system provides a useful and practical approximation for pre-flight evaluation compared to conventional planning methods that do not consider occlusions. Future work will focus on improving the robustness of the system by incorporating more detailed and up-to-date urban models, extending the framework to account for resolution, and supporting multi-sensor configurations and subsequent data-processing workflows such as DSM generation.

This contribution has been peer-reviewed. The double-blind peer-review was conducted on the basis of the full paper.
https://doi.org/10.5194/isprs-annals-XI-2-2026-419-2026 | © Author(s) 2026. CC BY 4.0 License.

References

Alfakhori, M., Dastageeri, H., Schneider, S., and Coors, V., 2022. Occlusion Screening Using 3D City Models as a Reference Database for Mobile AR-Applications, *ISPRS Ann. Photogramm. Remote Sens. Spatial Inf. Sci.*, X-4/W3-2022, 11–18, https://doi.org/10.5194/isprs-annals-X-4-W3-2022-11-2022, 2022.

Buyukdemircioglu, M. and Oude Elberink, S.,2024. Automated texture mapping CityJSON 3D city models from oblique and nadir aerial imagery, *ISPRS Ann. Photogramm. Remote Sens. Spatial Inf. Sci.*, X-4/W5-2024, 87–93, https://doi.org/10.5194/isprs-annals-X-4-W5-2024-87-2024, 2024.

Gajski, D., Dzięgielewska-Gajski, K., 2023. Nadir & Oblique Aerial Imagery – new possibilities in 3D mapping, *GIS Odyssey Journal*, 3(1), 137--147.

Ishikawa, M., Inazawa, T., Nakanishi, Y., Kawamata, F., Takada, M., Danjo, T., and Matsuoka, R., 2025. Resolution of a Texture Image Mapped on a Building Surface of a 3D City Model, *ISPRS Ann. Photogramm. Remote Sens. Spatial Inf. Sci.*, X-4/W6-2025, 89–96, https://doi.org/10.5194/isprs-annals-X-4-W6-2025-89-2025.

Leica Geosystems AG, 2025. Leica CityMapper-2, Leica CityMapper-2 DS.pdf, https://leica-geosystems.com/products/airborne-systems/hybrid-sensors/leica-citymapper-2

Matsuoka, R., Takemoto, T., Takahashi, G., Inazawa, T., and Sogo, S., 2024. A Novel Algorithm to Estimate Solar Irradiance of Urban Buildings for Photovoltaic Potential Estimation System Using a 3D City Model, *ISPRS Ann. Photogramm. Remote Sens. Spatial Inf. Sci.*, X-4/W4-2024, 115–122, https://doi.org/10.5194/isprs-annals-X-4-W4-2024-115-2024, 2024.

Minella, F., Rossi, F. A., Krüger, E., 2011. Analysis of the daytime effect of the sky view factor on the microclimate and on thermal comfort levels in pedestrian streets of Curitiba, *Ambiente Construído*, 11(1), 123-143.

Ministry of Land, Infrastructure, Transport and Tourism of Japan (MLIT), 2025. https://www.mlit.go.jp/plateau (April 7, 2025).

Vacca, G., Dessì, A., Sacco, A., 2017. The Use of Nadir and Oblique UAV Images for Building Knowledge, *ISPRS International Journal of Geo-Information*, 9(12), 393.

Vexcel Imaging GmbH, 2025. ULTRACAM EAGLE 4.1, https://www.vexcel-imaging.com/brochures/UC_Eagle_4.1_en.pdf